

Coulomb drag in graphene – boron nitride heterostructures: the effect of virtual phonon exchange

Bruno Amorim,¹ Jürgen Schiefele,² Fernando Sols,² and Francisco Guinea¹

¹*Instituto de Ciencia de Materiales de Madrid, CSIC, Cantoblanco, E-28 049, Madrid, Spain*

²*Departamento de Física de Materiales, Universidad Complutense de Madrid, E-28 040, Madrid, Spain*

(Dated: June 1, 2012)

We consider the drag effect between charge carriers in two spatially separated monoatomic graphene layers embedded in hexagonal boron nitride. Commonly, the phenomenon is described in terms of an interlayer Coulomb interaction. We show that if an additional electron – electron interaction via exchange of virtual substrate phonons is included in the model, the temperature dependence of the predicted drag resistivity is modified considerably at temperatures above 150 K. The anisotropic crystal structure of boron nitride, with strong intralayer and comparatively weak interlayer bonds, is found to play an important role in this effect.

I. INTRODUCTION

If two systems containing mobile charge carriers are spatially separated such that direct charge transfer is not possible, but close enough to allow interaction between the carriers in different layers, the resulting momentum transfer will equalize the drift velocities in both systems. This frictional effect was experimentally observed between (quasi) two-dimensional electron gases in double quantum well structures^{1,2}. In most of the theoretical work the interlayer interaction was attributed to Coulomb scattering, hence the effect now bears the name ‘Coulomb drag’ (see Refs. 3–5).

Interest in the subject has been revived recently by the experimental progress which made it possible to prepare two-dimensional electron systems based on monolayer graphene. A considerable number of theoretical works^{6–16} studied Coulomb drag between massless Dirac fermions, which effectively describe the charge carriers in graphene¹⁷. However, the experimental data published so far is still scarce^{18,19} and remains not satisfactorily explained by the existing theory⁶.

In the typical experiment, Coulomb drag is studied by driving a constant current I_2 through one of the layers (the active one, labeled by the index $\lambda = 2$ in Fig. 1). If no current is allowed to flow in the other (passive, index 1) layer, a potential difference V_1 builds up there. In terms of these two quantities, the drag resistivity $\rho_D \equiv (W/L)V_1/I_2$ serves as a measure of the momentum transfer between the two layers, where W and L are, respectively, the width and the length of the layer. A theoretical expression for ρ_D in second order in the interlayer interaction can be derived either using Boltzmann’s kinetic equation^{4,10,11,20} or the Kubo formula^{5,9,11}.

In the present work, we focus on the interlayer interaction responsible for the drag effect in heterostructures composed of two graphene monolayers and hexagonal boron nitride (hBN), see Fig. 1. The large bandgap insulator hBN is a piezoelectric isomorph to graphite. Recently the material received much attention as it allows the construction of graphene – hBN devices with, in comparison to the much used SiO₂ substrates, favorable

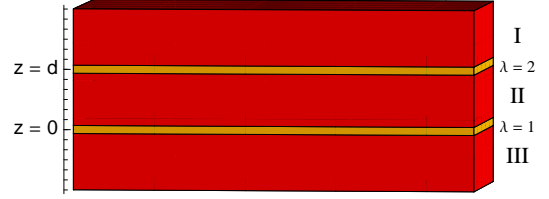


FIG. 1. A sketch of the double layer system under consideration. The two monoatomic graphene layers (yellow) with charge carrier concentration n_1 , n_2 are placed at $z = 0$ and $z = d$ and labeled by the layer index $\lambda = 1, 2$, respectively. The surrounding space (regions I, II, and III) is filled with the insulating material boron nitride (hBN).

high carrier mobilities^{21–24}. In particular, the Manchester group reported the fabrication of devices where a few layer thin hBN crystal, obtained by exfoliation, is sandwiched between two monolayers of graphene^{25–27}. If such a structure is used for a Coulomb drag experiment, the Dirac fermions in the active and passive layer can exchange momentum not only via Coulomb interaction but also by phonon exchange through the spacer medium. The effect of such a combined coupling on the drag resistivity has previously only been studied for quasi two dimensional electron gases in layered semiconductor systems^{28–32}.

In the following, we first investigate the effects of the anisotropy of hBN, where the bonds in between the graphene-like planes are much weaker than the in-plane bonds, on the electron – electron interaction via phonon exchange. We then show that the inclusion of phonon exchange into the description of Coulomb drag significantly alters the temperature dependence of the predicted value for ρ_D at temperatures above 150 K.

II. INTERLAYER INTERACTION

In a two-layer system as shown in Fig. 1, where the regions I, II and III are filled with a homogeneous isotropic dielectric medium, the interaction $U_{\lambda\lambda'}^{(0)}$, be-

tween electrons in layers λ and λ' via the combined effects of a static Coulomb potential and virtual substrate phonon exchange through the medium is of the form $e^2/[2q\epsilon_{\text{vac}}\epsilon(\omega)]\exp[-qd(1-\delta_{\lambda\lambda'})]$, where $\mathbf{q} = (q_x, q_y)$ is a two-dimensional momentum, ϵ_{vac} denotes the dielectric constant of vacuum and $\epsilon(\omega)$ the frequency dependent dielectric function of the medium^{28,30,31}.

In the anisotropic material hBN with its layered structure, the dielectric tensor $\epsilon(\omega)$ has two distinct eigenvalues³³: $\epsilon(\omega) = \text{diag}[\epsilon_{\text{in}}(\omega), \epsilon_{\text{in}}(\omega), \epsilon_{\text{out}}(\omega)]$, where $\epsilon_{\text{in/out}}$ refer to the dielectric function along the layer directions or perpendicular to them (that is, along the c -axis of the material, which coincides with the z direction). Both retarded³⁴ dielectric functions, ϵ_{in} and ϵ_{out} , of bulk hBN are of the form

$$\epsilon_{(\text{in/out})} = \epsilon_{\infty} + \sum_{i=1,2} f_i \frac{\omega_i^2}{\omega_i^2 - \omega^2 - i\gamma_i\omega}, \quad (1)$$

where the experimental values of the different parameters are listed in Table I. To obtain the interactions $U_{12}^{(0)} = -e\phi(q, d)$ and $U_{11}^{(0)} = U_{22}^{(0)} = -e\phi(q, 0)$ in the anisotropic medium, one has to solve Poisson's equation $-\nabla \cdot (\epsilon \cdot \nabla \phi) = \rho_{\text{free}}/\epsilon_{\text{vac}}$, (with ρ_{free} being the free charge density) for a point charge ($-e$) at the origin to obtain the Coulomb potential $\phi(\mathbf{q}, z)$. Poisson's equation becomes

$$-\frac{\partial}{\partial z} \left(\epsilon_{\text{out}} \frac{\partial}{\partial z} \phi(\mathbf{q}, z) \right) + q^2 \epsilon_{\text{in}} \phi(\mathbf{q}, z) = -\frac{e}{\epsilon_{\text{vac}}} \delta(z), \quad (2)$$

which finally results in the combined Coulomb-phonon interaction between electrons

$$U_{\lambda\lambda'}^{(0)}(q, \omega) = \frac{e^2}{2\epsilon_{\text{vac}}\epsilon_{\text{out}}(\omega)q} \sqrt{\frac{\epsilon_{\text{out}}(\omega)}{\epsilon_{\text{in}}(\omega)}} \times \exp \left[-qd(1 - \delta_{\lambda\lambda'}) \sqrt{\frac{\epsilon_{\text{in}}(\omega)}{\epsilon_{\text{out}}(\omega)}} \right]. \quad (3)$$

A generalization of this result to structures where the regions I, II, and III (see Fig. 1) are filled with different insulating materials (or air) is straightforward; $U_{11}^{(0)}$ then involves different dielectric functions than $U_{22}^{(0)}$.

To take into account the screening properties of the conduction electrons in the graphene layers themselves, we employ the standard procedure of solving the Dyson equation for the two-layer system within the RPA (see Ref. 5). This finally yields the dressed interlayer interaction

$$U_{21}(q, \omega) = \frac{U_{21}^{(0)}(q, \omega)}{\epsilon_{\text{RPA}}(q, \omega)}. \quad (4)$$

The total screening function for the coupled electron-phonon system given by³¹

$$\epsilon_{\text{RPA}} = (1 - U_{11}^{(0)}\chi_1)(1 - U_{22}^{(0)}\chi_2) - U_{12}^{(0)}U_{21}^{(0)}\chi_1\chi_2, \quad (5)$$

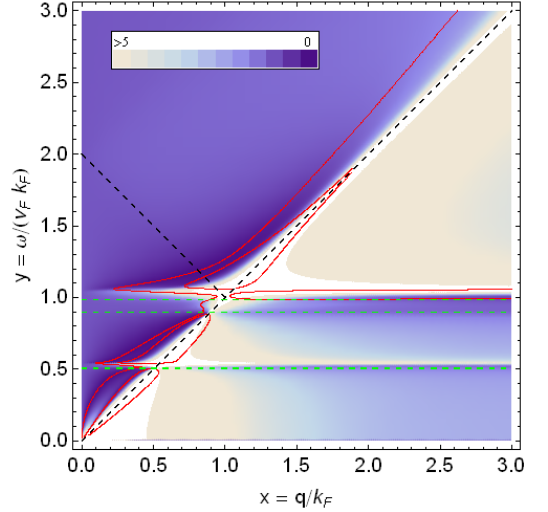


FIG. 2. Absolute value of the total screening function ϵ_{RPA} Eqn. (5), with $n_1 = n_2 = 0.02 \text{ nm}^{-2}$ and $d = 8 \text{ nm}$. Vertical green lines show the transverse optical resonance frequencies of hBN (see Table I), red curves mark the zeros of $\text{Re} \epsilon_{\text{RPA}}$. The dashed black lines show the line $y = x$ and mark the region where $\text{Im} \chi = 0$. The hybridization between phonon and plasmon modes is clear.

where $\chi_{1,2}$ denotes the (frequency and momentum dependent) polarizability of the graphene layers³⁵.

Fig. 2 shows a density plot of $|\epsilon_{\text{RPA}}(q, \omega)|$, using dimensionless units $x = q/k_F$ and $y = \omega/(v_F k_F)$, where k_F is the Fermi momentum. The horizontal dashed green lines mark the transverse optical resonance frequencies of hBN, where the dielectric function Eqn. (1) of the spacer material is close a pole. Near these frequencies, the absolute value of the total screening function ϵ_{RPA} likewise shows an abrupt change from high values (light colors) to almost zero (dark colors). In regions where $|\epsilon_{\text{RPA}}|$ is small, the red lines $\text{Re} \epsilon_{\text{RPA}} = 0$ show the coupled plasmon-phonon dispersion relation of the two-layer system.

III. RESULTS FOR THE DRAG RESISTIVITY

In the following, we assume for the sake of simplicity the same positive carrier density n (corresponding to electron doping) in both layers. The drag resistivity then assumes a negative value¹⁸. The first non-vanishing contribution to ρ_D obtained in perturbation theory is of second order in the dressed interlayer interaction^{4,5}. In terms of the variables carrier density, layer separation, and temperature, and under the assumptions that both layers are with high electron doping and $T \ll T_F$ ³⁶, it reads (refer to Refs. 6 and 10 for details)

$$\rho_D = -\frac{\hbar}{e^2} \frac{\alpha_g^2}{8} \frac{\hbar v_F \sqrt{\pi n}}{k_B T} \int_0^\infty dx \int_0^\infty dy \mathcal{K}(T, d, n), \quad (6)$$

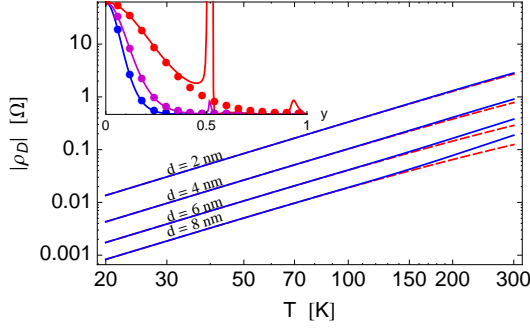


FIG. 3. Drag resistivity Eqn. (6) versus temperature for various interlayer distances, $n = 0.02 \text{ nm}^{-2}$. The blue curves include interaction via phonon exchange as in Eqn. (3), the dashed red curves consider Coulomb interaction only. The inset shows the integral kernel \mathcal{K} of Eqn. (7) with $x = q/k_F = 1$, $d = 8 \text{ nm}$, as a function of $y = \omega/v_F k_F$ for the temperatures 200, 100, 70 K (red, violet, blue from top to bottom). The dots show the same Kernel when only Coulomb interaction is considered.

where $\alpha_g = e^2/(4\pi\epsilon_{\text{vac}}v_F\hbar)$ denotes the effective fine structure constant in graphene and the integral kernel

$$\mathcal{K} = \frac{k_F^2 \epsilon_{\text{vac}}^2}{e^4} \frac{|U_{12}(x, y)|^2}{\sinh^2(y \frac{T_F}{2T})} \frac{x^7 \Phi^2(x, y)}{x^2 - y^2}. \quad (7)$$

The function Φ , defined in Eqn. (A1), is related to the nonlinear susceptibility of graphene, and restricts the integration range in the x, y -plane to the region $\omega < v_F q$.

The solid blue curves in Fig. 3 show the absolute value of ρ_D Eqn. (6) as a function of temperature, for fixed carrier concentration and different layer separations d . For comparison, the dashed red curves show the result obtained by considering only Coulomb interaction, that is, by substituting $U_{\lambda\lambda'}^{(0)}(q, \omega)$ with $U_{\lambda\lambda'}^{(0)}(q, 0)$ in the calculation of ρ_D , which is known to display an approximate T^2 behavior throughout the whole temperature range. At low temperatures, our full result Eqn. (6) does not differ from that obtained with Coulomb interaction only, but at large layer separations, the additional effect of virtual phonon exchange is seen to enhance the drag resistivity at temperatures higher than 150 K. For $d = 8 \text{ nm}$, the ratio between ρ_D with pure Coulomb interaction and ρ_D with combined Coulomb-phonon interaction is 0.93 at 150 K, 0.84 at 200 K, and 0.66 at room temperature, which can also be seen from the lowest (red) pair of dashed/full curves in Fig. 4. At $d = 2 \text{ nm}$, the ratio stays close to one up to room temperature, being 0.95 at 300 K.

The inset of Fig. 3 compares the integration kernel Eqn. (7) for fixed momentum $x = 1$ as a function of frequency (full lines) with the values obtained with Coulomb interactions only (dots). While both are almost identical at 70 K (lowest, blue line), the curves for 100 and 200 K (middle, violet and upper, red line) show additional peaks in the integrand near $y = 0.5$ and $y = 1$, which are due to phonon exchange (see Fig. 2).

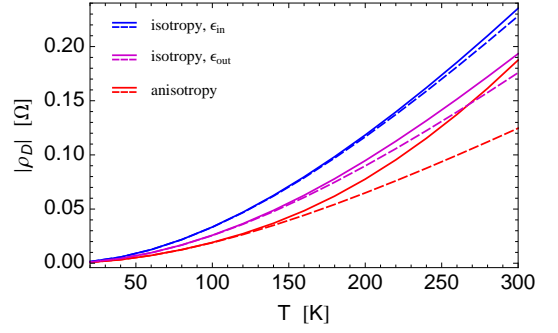


FIG. 4. Effect of the anisotropy of hBN in the behavior of drag with temperature. The parameters $n = 0.02 \text{ nm}^{-2}$, $d = 8 \text{ nm}$ were used. The curves *isotropy*, ϵ_{in} and *isotropy*, ϵ_{out} were computed assuming that the graphene layers are immersed in a isotropic dielectric medium, with dielectric functions given by ϵ_{in} and ϵ_{out} , respectively (Eqn. (1)). The curve *anisotropy* was computed taking into account the anisotropy of hBN Eqn. (3). Solid lines are for the case of static dielectric functions, while the dashed ones take into account the frequency dependence.

In Fig. 4 it is possible to see the effect of the anisotropy of hBN on the electron-electron interaction Eqn. (3). The greatest contribution comes from out-of plane phonons. (Note that the damping for this phonons is the lowest for the lower frequency resonance, see Table I.) Also notice that the mixed contribution from in plane and out of plane phonons causes a greater effect than the individual contributions.

TABLE I. Parameters for the dielectric function of hBN (see Eqn. (1)), taken from Ref. 33.

	E in plane	E out of plane
ϵ_∞	4.95	4.10
f_1	0.209	0.532
f_2	1.868	0.456
γ_1	4.35 meV	0.995 meV
γ_2	3.61 meV	9.95 meV
ω_1	95.4 meV	97.4 meV
ω_2	170 meV	188 meV

IV. SUMMARY AND DISCUSSION

We showed that including the electron – electron interaction via phonon exchange into the theory of Coulomb drag significantly changes the temperature dependence of the predicted drag resistivity in graphene-hBN heterostructures with layer separations greater than 4 nm: At temperatures higher than 150 K, ρ_D deviates from the T^2 dependence obtained in a calculation with Coulomb interaction only.

As the lowest phonon resonance frequency in the spacer

material hBN corresponds to a temperature of approximately 1100 K, our result at first sight seems to be at odds with the notion that phonon effects should be proportional to the thermal population factor of the relevant modes. This is indeed the case for other transport phenomena, like the substrate limited electron mobility in graphene, where real momentum transfer from an electronic state (in graphene) to a phonon mode (in a dielectric substrate material) plays a role^{23,37}. The decay rate of the electronic state is then overall proportional to the thermal population of the phonon mode. Our scenario however involves the exchange of virtual phonons in a process that is of second order in the interlayer interaction⁵, and no decay processes into real phonon states are relevant for ρ_D . We note that in Ref. 7, the effect of substrate phonons on Coulomb drag was considered for the case where a material described by a uniform dielectric function fills what is our region III of Fig. 1, and a deviation from the T^2 behavior of ρ_D was predicted for temperatures roughly an order of magnitude lower than the phononic resonance frequency of the substrate material.

Up to date, the considerable discrepancy between the only published experimental data on Coulomb drag between graphene layers^{18,19} (embedded in SiO₂) and the existing theory remains unresolved (see Ref. 6 for a detailed discussion). As hBN in general allows for the construction of much cleaner graphene based devices than other common substrate materials²¹, we think that future

experiments with devices as considered in the present work will be able to check our predictions on the temperature dependence of ρ_D .

ACKNOWLEDGMENTS

The authors would like to thank N.M.R. Peres for useful discussions. Financial support from Fundação para a Ciência e a Tecnologia (FCT) through Grant No. SFRH/BD/78987/2011 (B.A.), the Marie Curie ITN *NanoCTM* (J.S.) and from MICINN (Spain) through Grant No. FIS2010-21372 (F.S.) and FIS2008-00124 (F.G.) is acknowledged.

Appendix A: Mathematical details

The function $\Phi(x, y)$ appearing in Eqn. (7) reads^{6,10}

$$\begin{aligned} \Phi(x, y) = & \Phi^+(x, y) \Theta(y - x + 2) \Theta(x - y) \\ & + \Phi^-(x, y) \Theta(1 - y - |1 - x|), \end{aligned} \quad (\text{A1})$$

where

$$\Phi^\pm = \pm \cosh^{-1} \left(\frac{2 \pm x}{y} \right) \mp \frac{2 \pm x}{y} \sqrt{\left(\frac{2 \pm x}{y} \right)^2 - 1}.$$

-
- ¹ T. J. Gramila, J. P. Eisenstein, A. H. MacDonald, L. N. Pfeiffer, and K. W. West, Phys. Rev. Lett. **66**, 1216 (1991).
 - ² U. Sivan, P. M. Solomon, and H. Shtrikman, Phys. Rev. Lett. **68**, 1196 (1992).
 - ³ L. Zheng and A. H. MacDonald, Phys. Rev. B **48**, 8203 (1993).
 - ⁴ K. Flensberg, B. Y.-K. Hu, A.-P. Jauho, and J. M. Kinaret, Phys. Rev. B **52**, 14761 (1995).
 - ⁵ A. Kamenev and Y. Oreg, Phys. Rev. B **52**, 7516 (1995).
 - ⁶ B. Amorim and N. R. Peres, ArXiv e-prints (2012), 1203.6777.
 - ⁷ M. Carrega, T. Tudorovskiy, A. Principi, M. I. Katsnelson, and M. Polini, ArXiv e-prints (2012).
 - ⁸ M. I. Katsnelson, Phys. Rev. B **84**, 041407 (2011).
 - ⁹ B. N. Narozhny, M. Titov, I. V. Gornyi, and P. M. Ostrovsky, ArXiv e-prints (2011).
 - ¹⁰ N. M. R. Peres, J. M. B. L. dos Santos, and A. H. C. Neto, EPL (Europhysics Letters) **95**, 18001 (2011).
 - ¹¹ E. H. Hwang, R. Sensarma, and S. Das Sarma, Phys. Rev. B **84**, 245441 (2011).
 - ¹² W.-K. Tse, B. Y.-K. Hu, and S. Das Sarma, Phys. Rev. B **76**, 081401 (2007).
 - ¹³ S. M. Badalyan and F. M. Peeters, ArXiv e-prints (2012), 1204.4598.
 - ¹⁴ B. Scharf and A. Matos-Abiague, ArXiv e-prints (2012), 1204.3385.
 - ¹⁵ M. Schütt, P. M. Ostrovsky, M. Titov, I. V. Gornyi, B. N. Narozhny, and A. D. Mirlin, ArXiv e-prints (2012), 1205.5018.
 - ¹⁶ J. C. W. Song and L. S. Levitov, ArXiv e-prints (2012), 1205.5257.
 - ¹⁷ A. H. Castro Neto, F. Guinea, N. M. R. Peres, K. S. Novoselov, and A. K. Geim, Rev. Mod. Phys. **81**, 109 (2009).
 - ¹⁸ S. Kim, I. Jo, J. Nah, Z. Yao, S. K. Banerjee, and E. Tutuc, Phys. Rev. B **83**, 161401 (2011).
 - ¹⁹ S. Kim and E. Tutuc, Solid State Communications (2012), in press.
 - ²⁰ A.-P. Jauho and H. Smith, Phys. Rev. B **47**, 4420 (1993).
 - ²¹ R. C. Dean, A. F. Young, I. Meric, C. Lee, L. Wang, S. Sorgenfrei, K. Watanabe, T. Taniguchi, P. Kim, K. L. Shepard, et al., Nat Nano **5**, 722 (2010).
 - ²² A. S. Mayorov, R. V. Gorbachev, S. V. Morozov, L. Britnell, R. Jalil, L. A. Ponomarenko, P. Blake, K. S. Novoselov, K. Watanabe, T. Taniguchi, et al., Nano Letters **11**, 2396 (2011).
 - ²³ J. Schiefele, F. Sols, and F. Guinea, Phys. Rev. B **85**, 195420 (2012).
 - ²⁴ J. M. Garcia, U. Wurstbauer, A. Levy, L. N. Pfeiffer, A. Pinczuk, A. S. Plaut, L. Wang, C. R. Dean, R. Buizza, A. V. D. Zande, et al., Solid State Communications **152**, 975 (2012).
 - ²⁵ L. A. Ponomarenko, A. K. Geim, A. A. Zhukov, R. Jalil, S. V. Morozov, K. S. Novoselov, I. V. Grigorieva, E. H. Hill, V. V. Cheianov, V. I. Fal'ko, et al., Nat Phys **7**, 958 (2011).
 - ²⁶ L. Britnell, R. V. Gorbachev, R. Jalil, B. D. Belle, F. Schedin, A. Mishchenko, T. Georgiou, M. I. Katsnelson,

- L. Eaves, S. V. Morozov, et al., *Science* **335**, 947 (2012).
- ²⁷ L. Britnell, R. V. Gorbachev, R. Jalil, B. D. Belle, F. Schedin, M. I. Katsnelson, L. Eaves, S. V. Morozov, A. S. Mayorov, N. M. R. Peres, et al., *Nano Letters* **12**, 1707 (2012).
- ²⁸ R. Jalabert and S. Das Sarma, *Phys. Rev. B* **40**, 9723 (1989).
- ²⁹ H. C. Tso, P. Vasilopoulos, and F. M. Peeters, *Phys. Rev. Lett.* **68**, 2516 (1992).
- ³⁰ K. Güven and B. Tanatar, *Phys. Rev. B* **56**, 7535 (1997).
- ³¹ C. Zhang and Y. Takahashi, *Journal of Physics: Condensed Matter* **5**, 5009 (1993).
- ³² T. J. Gramila, J. P. Eisenstein, A. H. MacDonald, L. N. Pfeiffer, and K. W. West, *Phys. Rev. B* **47**, 12957 (1993).
- ³³ R. Geick, C. H. Perry, and G. Rupprecht, *Phys. Rev.* **146**, 543 (1966).
- ³⁴ We are here using the retarded expression (defined as being analytic in the upper half of the complex ω plane) in order to be consistent with the likewise retarded polarizability taken from Ref. 38. Not keeping this consistency yields significantly different results.
- ³⁵ In the numerical calculations, we use for simplicity the zero temperature expression for χ as calculated in Refs. 38 and 39, which is a good approximation for $T \ll T_F$, with T_F the Fermi temperature.
- ³⁶ We here use a simplified form of the nonlinear susceptibility of graphene, which is valid for electron doping high enough such that the existence of the valence band can be ignored. The condition $T \ll T_F$ is important as we use the zero temperature expressions for the polarizability of graphene. See Refs. 6 and 10 for a discussion of both approximations.
- ³⁷ S. Fratini and F. Guinea, *Phys. Rev. B* **77**, 195415 (2008).
- ³⁸ B. Wunsch, T. Stauber, F. Sols, and F. Guinea, *New Journal of Physics* **8**, 318 (2006).
- ³⁹ E. H. Hwang and S. Das Sarma, *Phys. Rev. B* **75**, 205418 (2007).